Time-dependent Hartree-Fock calculations of $^4He+^{14}C$, $^{12}C+^{12}C(0^+)$, and $^4He+^{20}Ne$ molecular formations

A. S. Umar
Wright Nuclear Structure Laboratory, Department of Physics, Yale University, New Haven, Connecticut 06511 and Physics Division, Oak Ridge National Laboratory, Oak Ridge, Tennessee 37831

M. R. Strayer
Physics Division, Oak Ridge National Laboratory, Oak Ridge, Tennessee 37831

R. Y. Cusson
Department of Physics, Duke University, Durham, North Carolina 27706

P.-G. Reinhard*
Physics Division, Oak Ridge National Laboratory, Oak Ridge, Tennessee 37831

D. A. Bromley
Wright Nuclear Structure Laboratory, Department of Physics, Yale University, New Haven, Connecticut 06511
(Received 17 December 1984)

Time-dependent Hartree-Fock calculations for head-on collisions of $^4He+^{14}C$, $^{12}C+^{12}C(0^+)$, and $^4He+^{20}Ne$ have been performed at bombarding energies near the Coulomb barrier. The results are interpreted in terms of their classical quasiperiodic and chaotic behavior. The position of the time-dependent Hartree-Fock collective path with respect to the multidimensional energy surface of the compound nuclear system is shown. Dynamical collective degrees of freedom are identified and classical frequencies associated with each degree of freedom are calculated. For ^{24}Mg we calculate molecular frequencies of about 0.8 and 1.0 MeV and a characteristic moment of inertia of 15 MeV^{-1}.

I. INTRODUCTION

In recent years considerable progress has been made in the study of large amplitude collective phenomena. The time-dependent Hartree-Fock (TDHF) theory[1-7] constitutes a well-defined starting point for the study of such motion. The usual TDHF approximation yields a classical or semiclassical description of the collective motion. Theories attempting to achieve some form of a quantized TDHF theory include adiabatic time-dependent Hartree-Fock theory (ATDHF),[8-13] the generator coordinate method (GCM),[14] the time-dependent GCM,[15] and the functional integral theories which formulate the bound state of a many-body system and collective energies in terms of periodic TDHF solutions.[16-20] The ATDHF and GCM theories require a restriction to one or more collective coordinates. Although the functional integral methods are free of any such conceptual difficulties, numerical solutions of the resulting equations are presently not possible.

In the present work, we study quasiperiodic TDHF solutions using the TDHF formalism.[1-7] The long-time motion of the collective nuclear coordinates are analyzed in terms of their classical quasiperiodic and chaotic behavior. Chaos[21] concerns the long-time behavior of nonintegrable mechanical systems and addresses questions as to the nature of energy dissipation and equilibration of energy. These ideas were first used, within the context of nuclear physics, by Fermi, Pasta, and Ulam.[22] In present-day nuclear physics, the long-time classical behavior arises through various limits of the nuclear many-body state, as in the TDHF studies of heavy-ion reactions, the nuclear partition function,[23] fission lifetimes,[17] and S-matrix elements.[24] Similarly, the hydrodynamic models of heavy-ion reactions exhibit dissipative fluid flow behavior,[25] where the details of the momentum transfer and particle multiplicities may be evidence for the formation of attractor regions in the reaction phase space.[26] On the other hand, in the small amplitude limit, quasiperiodic TDHF solutions yield unquantized vibrational frequencies, with the classical interpretation of being the most probable random phase approximation (RPA) frequencies. In this context, TDHF calculations of isoscalar and isovector, monopole and quadrupole, giant resonances have been found to be in good agreement with both RPA and GCM results.[27]

We obtain quasiperiodic TDHF solutions by initiating head-on collisions with bombarding energies near the Coulomb barrier. The initial energy and the separation of the centers of the ions are parameters labeling the initial state. The initial energy is varied until a quasiperiodic solution is found. From these solutions, the important collective degrees of freedom are identified and the associated classical frequencies are calculated. We also calculate a multidimensional energy surface along the TDHF path using the density constrained Hartree-Fock (DCHF) method.

In the next section we briefly describe the TDHF for-

malism used in our study. Section III examines the quasiperiodic TDHF results for systems ^{4}He+^{14}C, ^{12}C+^{12}C(0$^+$), and ^{4}He+^{20}Ne. In Sec. IV we examine the long-time behavior from the point of view of chaos. The paper is concluded with a summary of the results. Some of these results have been previously published.[28–30]

II. FORMALISM

In this section we give a brief description of the TDHF formalism and discuss some of the numerical methods utilized in these calculations. A more detailed description of the TDHF theory is available in the literature.[1–7] The TDHF equations can be obtained from the variation of the many-body action S,[1]

$$S=\int_{t_1}^{t_2} dt \langle \psi(t) \mid i\partial_t - H \mid \psi(t) \rangle \ . \tag{1}$$

In this expression the many-body Hamiltonian H is given by,

$$H=\sum_{i=1}^{A} T_i + \tfrac{1}{2}\sum_{i,j=1} V_{ij} + \frac{1}{3!}\sum_{i,j,k=1}^{A} V_{ijk} \ , \tag{2}$$

where T is the one-body kinetic energy operator and the potential terms represent two- and three-body interactions. The A-nucleon wave function $\Psi(t)$ is chosen to be of determinantal form, constructed from the time-dependent single-particle states $\psi_\lambda(t)$,

$$\Psi(\mathbf{r}_i, \ldots, \mathbf{r}_A; t)=\frac{1}{\sqrt{A!}}\det||\Psi_{\lambda_i}(\mathbf{r},t)|| \ . \tag{3}$$

The variation of Eq. (1) is an independent variation with respect to the single-particle states ψ_λ and ψ_λ^* and yields the equations of motion,

$$i\dot{\psi}_\lambda(\mathbf{r},t)=\frac{\delta\langle H\rangle}{\delta\psi_\lambda^*(\mathbf{r},t)}\equiv h(\mathbf{r},t)\psi_\lambda(\mathbf{r},t) \tag{4}$$

and a similar equation for $\psi_\lambda^*(\mathbf{r},t)$. The classical nature of these equations can be put into a better perspective via the definition of classical field coordinates $\phi_\lambda(\mathbf{r},t)$, and conjugate momenta $\pi_\lambda(\mathbf{r},t)$,

$$\begin{aligned} \phi_\lambda &= (\psi_\lambda+\psi_\lambda^*)/\sqrt{2} \ , \\ \pi_\lambda &= (\psi_\lambda-\psi_\lambda^*)/\sqrt{2}\,i \ . \end{aligned} \tag{5}$$

The result is then the Hamilton's equations,

$$\begin{aligned} \dot{\phi}_\lambda(\mathbf{r},t) &= \delta\langle H\rangle/\delta\pi_\lambda(\mathbf{r},t) \ , \\ \dot{\pi}_\lambda(\mathbf{r},t) &= -\delta\langle H\rangle/\delta\phi_\lambda(\mathbf{r},t) \ . \end{aligned} \tag{6}$$

The TDHF equation (4) and its complex conjugate are solved on a three-dimensional space-time lattice[5] with initial wave functions of the form,

$$\begin{aligned} \lim_{t\to-\infty} \phi_\lambda(\mathbf{r},t) &\to \sqrt{2}\cos(\mathbf{k}_\lambda\cdot\mathbf{r}-\epsilon_\lambda t)\chi_\lambda(\mathbf{r}-\mathbf{k}_\lambda/mt-\beta_\lambda) \ , \\ \lim_{t\to-\infty} \pi_\lambda(\mathbf{r},t) &\to \sqrt{2}\sin(\mathbf{k}_\lambda\cdot\mathbf{r}-\epsilon_\lambda t)\chi_\lambda(\mathbf{r}-\mathbf{k}_\lambda/mt-\beta_\lambda) \ , \end{aligned} \tag{7}$$

where χ_λ is the solution of the static Hartree-Fock equations,

$$h\chi_\lambda(\mathbf{r})=\epsilon_\lambda\chi_\lambda(\mathbf{r}), \quad \lambda=1,\ldots,A \tag{8}$$

and $\mathbf{k}_\lambda$ and $\boldsymbol{\beta}_\lambda$ are parameters of the initial boost.

In this work we solve Eq. (4) employing axial symmetry in cylindrical polar coordinates.[5] The ions are initially separated by a distance R, and their initial relative kinetic energy is denoted by E. During the time evolution, we examine both the isoscalar ($I=0$) and isovector ($I=1$) densities,

$$\hat{\rho}_I(\mathbf{r})=\sum_{\lambda=1}^{A}\delta(\mathbf{r}-\mathbf{r}_\lambda)\hat{a}_I(\lambda) \ ,$$

where

$$\langle q \mid \hat{a}_I \mid q' \rangle = \begin{cases} \delta_{qq'}, & q=\text{ proton} \\ (-1)^I\delta_{qq'}, & q=\text{ neutron.} \end{cases}$$

In terms of these quantities the density can be written as,

$$\rho_I(\mathbf{r},t)=\begin{cases} \rho_p(\mathbf{r},t)+\rho_n(\mathbf{r},t) & I=0 \\ \rho_p(\mathbf{r},t)-\rho_n(\mathbf{r},t) & I=1. \end{cases} \tag{9}$$

The densities ρ_p and ρ_n, in terms of the field coordinates and momenta, are

$$\rho_q(\mathbf{r},t)=\tfrac{1}{2}\sum_\lambda [\ |\pi_{\lambda,q}(\mathbf{r},t)|^2+|\phi_{\lambda,q}(\mathbf{r},t)|^2] \ ,$$

$$q=\mathrm{p,n} \ .$$

In our static and dynamic calculations we have used the finite-range Bonche-Koonin-Negele (BKN) force without any spin-orbit interaction. The numerical solution of Eq. (8) was performed, in coordinate space, using the gradient iteration method.[31] This method is similar to the imaginary time method,[32] and is discussed in Appendix A. The density constrained Hartree-Fock[33] method is essential for the calculation of the energy surface along the TDHF path. The details of this method are given in Appendix B.

We also calculate the classical electromagnetic radiation from the quasiperiodic charge distributions. The classical treatment of the radiation field results in a continuous spectrum, which is related to the time dependence of the moments of the proton density. We write the total action for the system as,

$$S=S_N+S_{\mathrm{EM}}+S_I \ . \tag{10}$$

In this expression S_N is the nuclear action given by Eq. (1), S_{EM} is the classical action for the free electromagnetic field, and S_I represents the action for the coupling of nuclear and electromagnetic parts.[34] In Gaussian units,

$$\begin{aligned} S_{\mathrm{EM}} &= -\frac{1}{16\pi}\int d^4x\, F_{\mu\nu}F^{\mu\nu} \ , \\ S_I &= -\frac{1}{c}\int d^4x\, A_\mu J^\mu \ , \end{aligned} \tag{11}$$

with

$$d^4x=dt\,d^3r \ .$$

In Eq. (11) the electromagnetic tensor $F_{\mu\nu}$ is defined as in Ref. 34, A_μ is a four-vector having its time component as the scalar potential ϕ and space component as the vector potential $\mathbf{A}$,

$$A^{\mu}=(\phi,\mathbf{A}) .$$

Similarly, the current four-vector is defined as,

$$J^{\mu}=(c\rho_{\rm p},\mathbf{J}_{\rm p}) ,$$

where $\mathbf{J}_{\rm p}(\mathbf{r},t)$ is the nuclear current,

$$\mathbf{J}_{\rm p}(\mathbf{r},t)=\sum_{\lambda\epsilon{\rm p}}{\rm Im}[\psi^{*}_{\lambda}(\mathbf{r},t)\nabla\psi_{\lambda}(\mathbf{r},t)] . \tag{12}$$

The variation of this action with respect to the single-particle states yields the equations of motion (4) plus a term coming from the variation of S_I, which we neglect. The variation of S in Eq. (10) with respect to fields A_{μ}, which, together with gauge invariance and current conservation, yields the four Maxwell equations in the presence of sources.

$$\begin{aligned}
&\nabla\times\mathbf{B}(\mathbf{r},t)=\frac{1}{c}\frac{\partial E}{\partial t}+\frac{4\pi}{c}\mathbf{J}_{\rm p}(\mathbf{r},t) ,\\
&\nabla\cdot\mathbf{E}(\mathbf{r},t)=4\pi\rho_{\rm p}(\mathbf{r},t) ,\\
&\nabla\times\mathbf{E}(\mathbf{r},t)=-\frac{1}{c}\frac{\partial\mathbf{B}}{\partial t} ,\\
&\nabla\cdot\mathbf{B}=0 .
\end{aligned} \tag{13}$$

With the definition of the Fourier transform,

$$\rho_{\rm p}(\mathbf{r},t)=\int_{-\infty}^{+\infty}\frac{d\omega}{2\pi}\exp(-i\omega t)\rho_{\rm p}(\mathbf{r},\omega)$$

and a similar expression for $\mathbf{J}_{\rm p}(\mathbf{r},t)$, these equations for each frequency component become,

$$\begin{aligned}
&\nabla\cdot\mathbf{B}(\mathbf{r},\omega)=0 ,\\
&\nabla\times\mathbf{E}(\mathbf{r},\omega)=i\omega/c\mathbf{B}(\mathbf{r},\omega) ,\\
&\nabla\cdot\mathbf{E}(\mathbf{r},\omega)=4\pi\rho_{\rm p}(\mathbf{r},\omega) ,\\
&\nabla\times\mathbf{B}(\mathbf{r},\omega)+\frac{i\omega}{c}\mathbf{E}(\mathbf{r},\omega)=\frac{4\pi}{c}\mathbf{J}_{\rm p}(\mathbf{r},\omega) .
\end{aligned} \tag{14}$$

The asymptotic solution of Eqs. (14) can be obtained[35] as,

$$\begin{aligned}
&\mathbf{B}(\mathbf{r},\omega)=\frac{e^{ikr}}{kr}\sum_{LM}(-i)^{L+1}a(L,M,\omega)\mathbf{L}Y_{LM}(\theta,\phi) ,\\
&\mathbf{E}(\mathbf{r},\omega)=\mathbf{B}(\mathbf{r},\omega)\times\hat{\mathbf{e}}_{\rm r} ,
\end{aligned} \tag{15}$$

where

$$a(L,M,\omega)=\frac{4\pi}{i(2L+1)!!}\left[\frac{L+1}{L}\right]^{1/2}\left[\frac{\omega}{c}\right]^{L+2}\times\int_{-\infty}^{+\infty}dt\exp(i\omega t)\int d^3r\, r^{L}Y_{LM}\rho_{\rm p}(\mathbf{r},t) .$$

The expression for the total radiated energy, integrated over a spherical surface at an asymptotic distance,

$$\begin{aligned}
W_{\rm tot}&=\int d\omega\, d\Omega\frac{d^2W}{d\omega\, d\Omega}\\
&=\int d\omega\, d\Omega\frac{c}{8\pi^2}\mathbf{E}^{*}(\mathbf{r},\omega)\times\mathbf{B}(\mathbf{r},\omega)\cdot\hat{\mathbf{e}}_{\rm r}r^2 ,
\end{aligned}$$

allows us to calculate the γ yield as a function of the energy $\hbar\omega$ as,

$$\frac{dN_{\gamma}}{dE}=\frac{\hbar c}{8\pi^2}\frac{1}{\hbar^3\omega^3}\sum_{L}(2L+1)\,|\,a(L,\hbar\omega)\,|^{2} . \tag{16}$$

III. QUASIPERIODIC SOLUTIONS

The TDHF equations (4) were used to study the long-time behavior of the ^{4}He+^{14}C reaction.[29]. The initial ^{14}C nucleus was obtained as a spherical approximation to the ground state using the filling approximation. The initial separation and the c.m. kinetic energy were 15 fm and 7.5 MeV, respectively. After the initial contact about 40 fm/c, the system relaxes into a configuration, undergoing quasiperiodic motion. In Fig. 1 we show the evolution of the density at various times. In a schematic interpretation the density shows an alpha particle and a ^{14}C nucleus which are exchanging about the center of mass of the ^{18}0 system. Figures 2 and 3 show the time and frequency dependence of the isoscalar quadrupole and octupole moments and the isovector dipole moment. The definitions of the moments are as follows:

$$\begin{aligned}
&M_{LI}(t)=\int d^3r\, r^{L}Y_{LM}(\hat{\mathbf{r}})\rho_{I}(\mathbf{r},t) ,\\
&M_{LI}(\omega)=\int_{-\infty}^{+\infty}dt\exp(-i\omega t)M_{LI}(t) .
\end{aligned} \tag{17}$$

We observe oscillations for times longer than the typical nuclear reaction times, with a relatively pure 4-MeV frequency in the isoscalar octupole mode, and 8- and 15-MeV frequencies in the isoscalar quadrupole mode. The isovector dipole mode has 4- and 9-MeV frequencies. The 4-MeV frequency may be due to the coupling of the isoscalar octupole and isovector dipole channels. A similar collision study was carried out for the ^{12}C+^{12}C(0$^+$) system. The ions were initially 12 fm apart with a c.m. kinetic energy of 7.5 MeV. The ^{12}C(0$^+$) initial configuration is obtained as a shape isomer with an apparent alpha cluster structure, as shown in Fig. 4. This state is a solution of the unconstrained Hartree-Fock equations and its choice follows from the supposition that it may represent

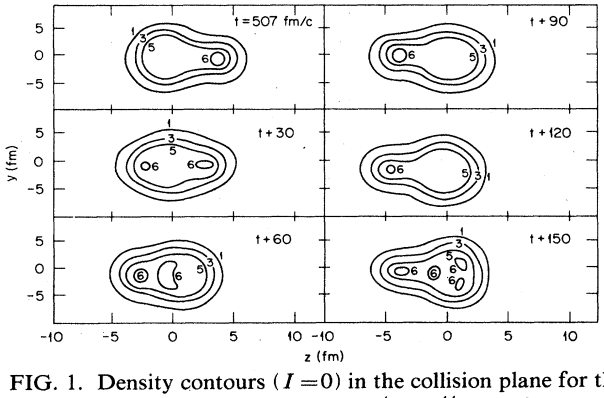

FIG. 1. Density contours ($I=0$) in the collision plane for the ^{18}O system, starting from the initial ^{4}He+^{14}C configuration. The times are considerably after the initial contact and exhibit the quasiperiodicity of the system. The density contours 1, 3, 5, and 6 are, respectively, 0.028, 0.084, 0.14, and 0.168 nucleons/fm^3.

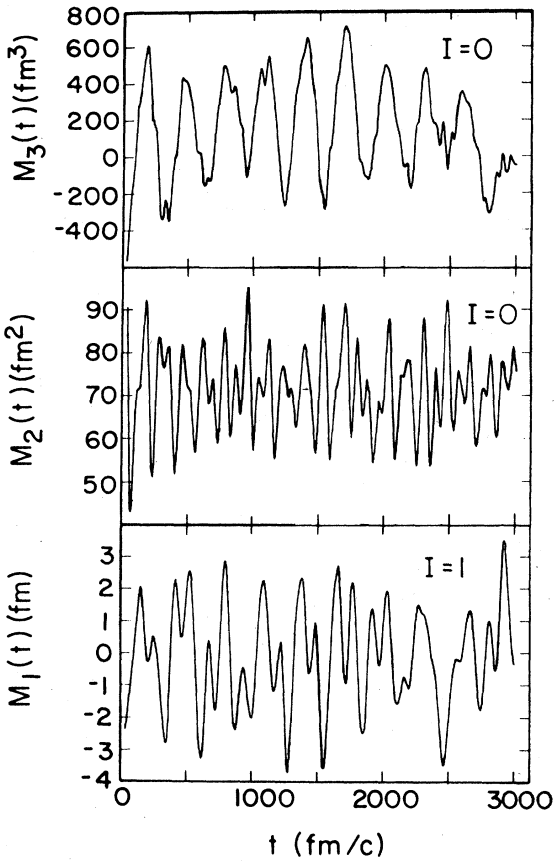

FIG. 2. The time dependence of the isoscalar octupole, isoscalar quadrupole, and the isovector dipole moments for the ^{18}O system.

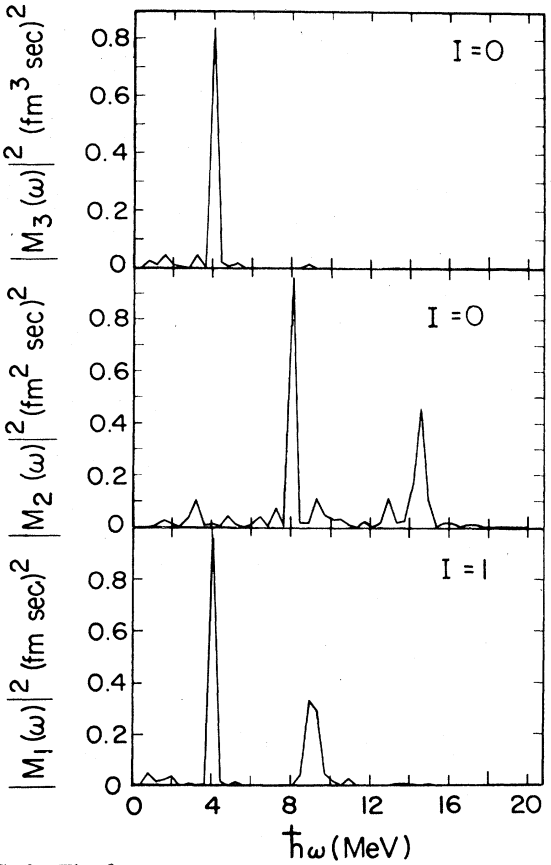

FIG. 3. The frequency dependence of the isoscalar octupole, isoscalar quadrupole, and the isovector dipole moments for the ^{18}O system.

one of the building blocks of the $^{12}C+^{12}C$ molecule.[36] Figure 4 shows the evolution of the isoscalar density at various times, and again, we see the quasiperiodic motion arising from a complicated matter flow. The Coulomb force induces rapid isovector density variations in time with a high multipole structure as shown in Fig. 5. The associated time dependence of the moments are shown in Fig. 6, while the frequency spectra are given in Fig. 7. Although the time and frequency dependence of the ^{18}O and ^{24}Mg systems seem qualitatively similar, they are quantitatively different. The time dependence of the isoscalar octupole moment is regular and corresponds to about a 1.5-MeV frequency. As before, the isoscalar quadrupole motion is a combination of low (2.5-MeV) and high (8-MeV) frequency motion. A similar calculation for the $^{4}He+^{20}Ne$ system with a kinetic energy of 6.5 MeV yields the frequency spectrum shown in Fig. 8. The similarities between the $^{12}C+^{12}C(0^+)$ and $^{4}He+^{20}Ne$ spectra, at these energies, indicate that both reactions are probing the same part of the ^{24}Mg collective energy surface.

In order to understand the TDHF evolution for these systems, we have computed the energy surfaces of ^{18}O and ^{24}Mg systems using DCHF calculations along the TDHF path. In a DCHF calculation, the isoscalar density is kept fixed while its energy is minimized to obtain the associated collective energy. In Figs. 9 and 10 we show the collective energy surfaces for ^{18}O and ^{24}Mg systems, respectively. The contours are in the collective subspace of the isoscalar quadrupole and octupole degrees of freedom. The isomers are 13 MeV higher than the ground state in the ^{18}O system and 36 MeV higher in the ^{24}Mg system. The time history of the TDHF evolution along the energy surface of Fig. 9 is as follows. The system starts with collective coordinates $q_2=1.7q_{20}$ and $q_3=-2.5q_{30}$, and it quickly evolves into the region shown in Fig. 9. The minimum energy E_0 in Fig. 9 is an axially symmetric shape isomer of the ^{18}O system and is a stable solution of the unconstrained Hartree-Fock minimization. The path for ^{24}Mg starts from the initial point $q_2=1.5q_{20}$ and $q_3=2.9q_{30}$ and transverses a complex path about the shape isomer with energy $E_0=-143.8$ MeV. The axially symmetric ground state of ^{24}Mg occurs at $q_2=42.3$ fm^2, with an energy of -179.7 MeV. These results are in agreement with other methods.[37]

IV. CHAOS

The approach of classical systems to chaos has been used to address a large class of problems in various fields of science.[38–40] In our discussions we follow the general

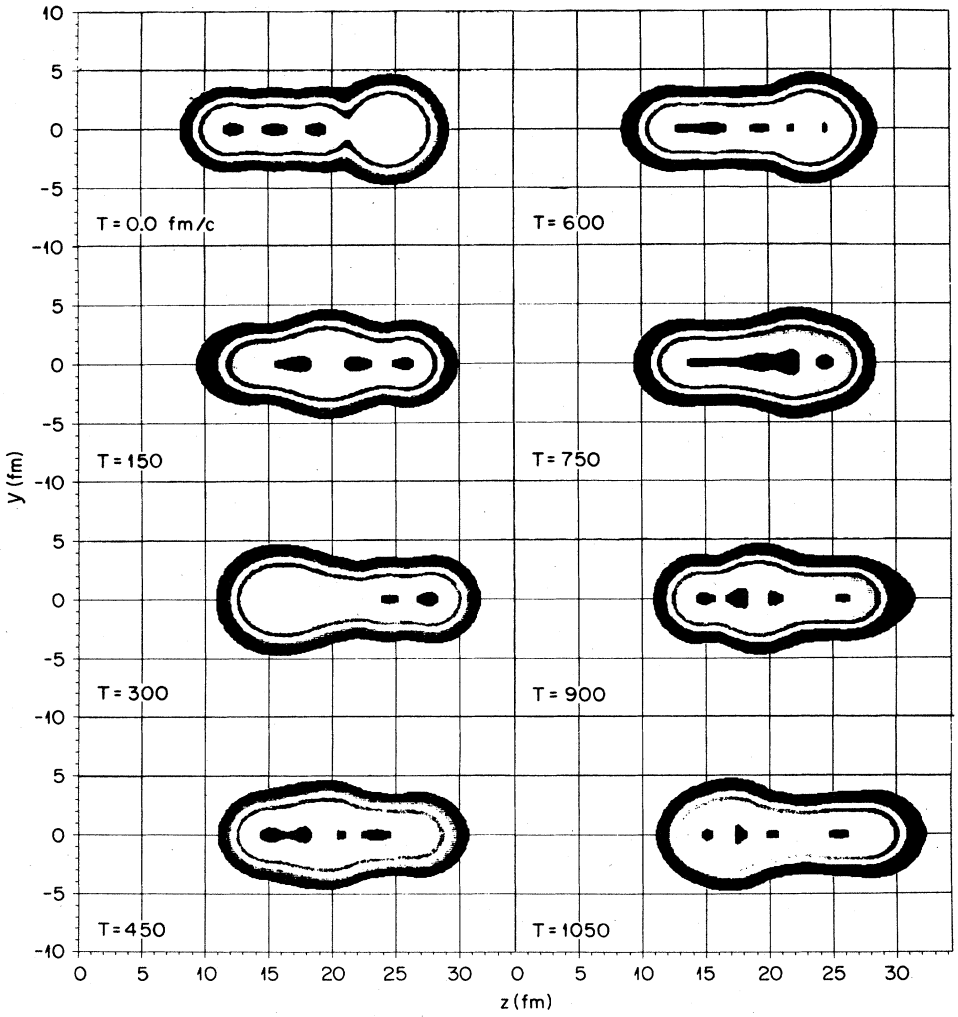

FIG. 4. Density contours ($I=0$) in the collision plane for the ^{24}Mg system, starting from an initial $^{12}C+^{12}C(0^+)$ configuration. Different times exhibit the quasiperiodicity of the system. The outer dark contour corresponds to 9×10^{-4}, the adjacent grey contour to 3×10^{-3}, the adjacent white contour to 8×10^{-3}, the adjacent grey contour to 3×10^{-2}, the adjacent white area to 7.2×10^{-2}, and the central dark region to 1.5×10^{-1} nucleons/fm^3.

methods of Ref. 41. They study a variety of requantization schemes for the classical trajectories of a three-level SU(3) model.[42] For this model, exact quantum-mechanical, as well as closed-form TDHF solutions, can be obtained. Upon classifying the motion to be one of the following three types: (a) periodic, (b) quasiperiodic, and (c) stochastic, they conclude that it is not possible to requantize stochastic motions, whereas the various requantization methods for the quasiperiodic motion all give reasonable results.

In order to interpret our results from the point of view of these conclusions, we plot the Poincaré projects for the motion of ^{24}Mg in Fig. 11. The velocity of the moments $\dot{M}_{LI}(t)$ in Fig. 11 were obtained from the knowledge of $M_{LI}(t)$ by using a first-order finite-difference expression. We see that both the isoscalar quadrupole and octupole modes seem to be filling most of the available phase space. The corresponding autocorrelation functions (Fig. 12),

$$C_{LI}(t)=\int_{-\infty}^{+\infty}\frac{d\omega}{2\pi}\exp(+i\omega t)\,|\,M_{LI}(\omega)\,|^2\,,$$

are small for all of the relevant modes suggesting that the motion is closer to being stochastic rather than periodic. These conclusions can be summarized as follows. The initial TDHF trajectory quickly relaxes into a region about the shape isomeric minimum and undergoes a complex, nonlinear quasiperiodic motion. To improve the degree of periodicity, the system must oscillate in the close neighborhood of the isomer. In practice, this can be achieved by localizing the TDHF trajectory via a DCHF minimization to the close neighborhood of this minimum. To test this idea, we start the evolution of the $^{12}C+^{12}C(0^+)$ system from the same initial conditions and follow the evolution until the system reaches a point in the vicinity of this minimum (in this case, about 700 fm/c). We then "cool" the system by keeping the density (or shape) fixed and minimizing the energy. The following evolution starts

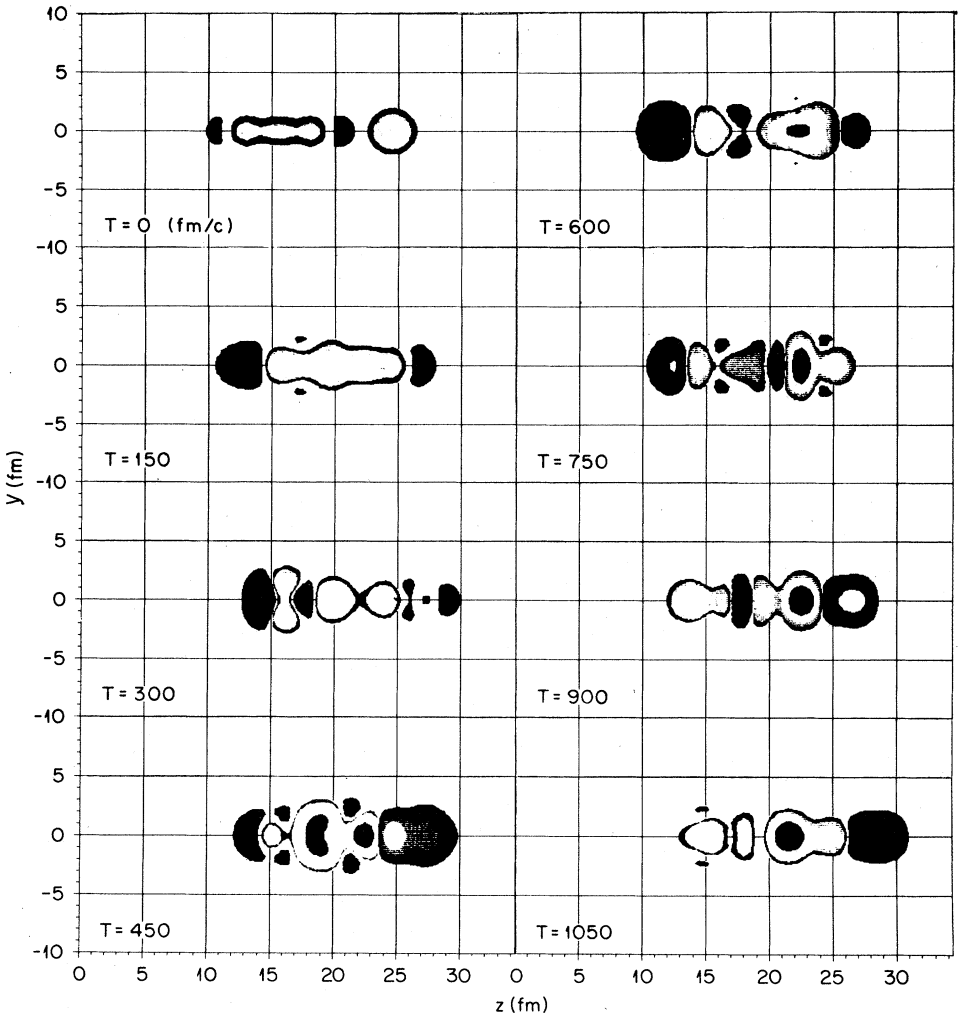

FIG. 5. Density contours ($I=1$) in the collision plane for the ^{24}Mg system, starting from an initial $^{12}C + {}^{12}C(0^+)$ configuration. The isovector densities change more rapidly in time, and they correspond to high multipole structures. The darkest contour corresponds to 8.8×10^{-4}, the grey contour always circled by the darkest contour to 3×10^{-3}, the isolated grey contours to -6×10^{-3}, the white regions to -4.4×10^{-3}, and the grey contours encircled by the white region to $-1.0\times10^{-2}\ e^2/\text{fm}^3$.

from this state. The time and frequency dependence of the isoscalar moments are shown in Fig. 13 and 14, respectively. The time dependence of the isoscalar moments are more periodic than the previous calculations; furthermore, the dominant low frequency of the motion now appears in all of these moments, which must be the case for exact periodicity. This trend also continues for odd isovector moments shown in Fig. 15 and 16. The even multipoles no not have the correct low-frequency behavior and they appear chaotic. Unlike Fig. 12, the autocorrelation functions (Fig. 17) for the isoscalar and odd-parity isovector modes show strong correlations in time.

The spectrum for the classical electromagnetic radiation, generated by the oscillating proton density of the cooled system, can be calculated from Eq. (16). The magnitude of the spectra fall rapidly with increasing values of L. Figure 18 shows this spectra for the dipole, quadrupole, and the octupole modes.

V. CONCLUSIONS

We have studied the collective motion of the ^{18}O and ^{24}Mg systems using the TDHF formalism. The reaction-like entrance channels were chosen to be appropriate for the study of nuclear molecules. We have tried to classify the TDHF collective paths in terms of their chaotic and quasiperiodic behavior. Even though the trajectory is focused into the reaction phase space of the isomer, the motion along the path appears stochastic and may be reflecting formation of a strange attractor near the shape isomeric minima. The motion approaches the chaotic region, although the TDHF path is found to be in the vicinity of the shape isomeric minimum. For ^{24}Mg, we have employed the DCHF method to cool the motion, and this resulted in quasiperiodic motion which was approximately harmonic. These results are important from the point of view that the quasiperiodic motion represents a known classical limit of quantum mechanics, whereas the sto-

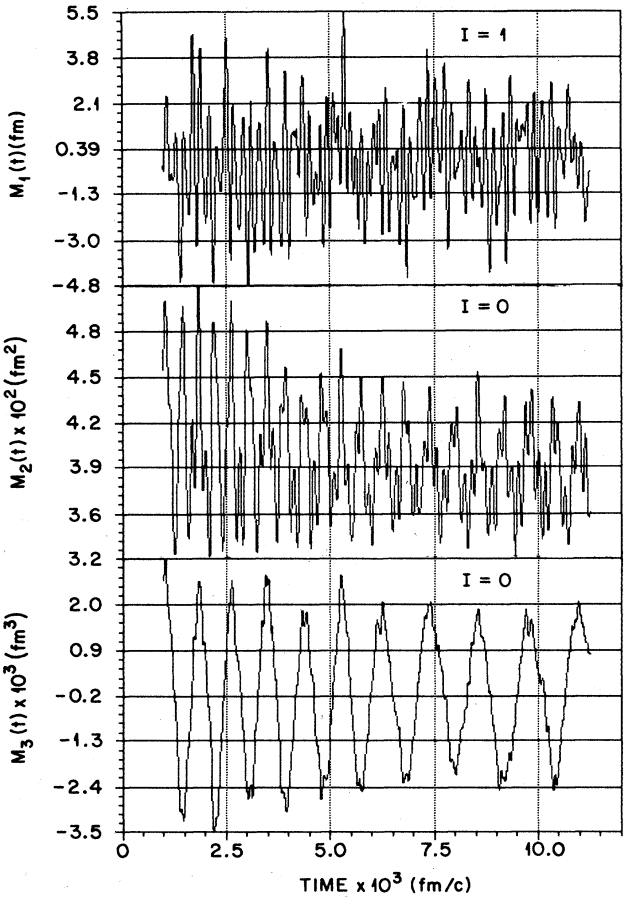

FIG. 6. The time dependence of the isovector dipole, isoscalar quadrupole, and the isoscalar octupole moments for the ^{24}Mg system.

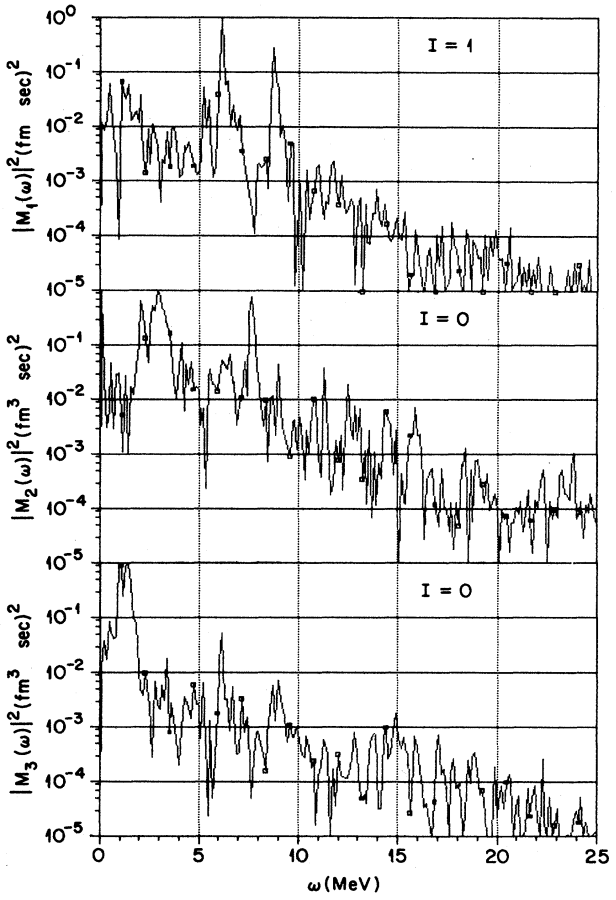

FIG. 7. The frequency dependence of the isovector dipole, isoscalar quadrupole, and the isovector octupole moments for the ^{24}Mg system.

chastic motion does not.[41] Although the memory of the initial alpha clustering seems to persist throughout the time evolution of these systems, it would not be appropriate to associate the molecular phenomena to a pure entrance-channel alpha-particle description.

Our calculations suggest the existence of highly collective structures of a giant resonance nature having compound nuclear properties at excitation energies of 13 MeV in ^{18}O and 36 MeV in ^{24}Mg. The characteristic low-lying vibrational frequencies in the isomer are approximately 0.8 MeV for odd-L and 1.0 MeV for even-L, with a moment of inertia of 15 MeV^{-1}. The isomer structure is 36 MeV above the ground state in ^{24}Mg and 13 MeV above the ground state in ^{18}O. The general features of the energy surface also agree with the Nilsson-Strutinsky calculations of Ref. 37.

ACKNOWLEDGMENTS

The research was sponsored in part by the U.S. Department of Energy under contract DE-AC02-ER03074 and under Contract DE-AC05-84OR21400 with Martin Marietta Energy Systems, Inc.

APPENDIX A

In this appendix we will outline the gradient iteration method[31] for solving the static Hartree-Fock equations (8). Unlike Ref. 31, here we choose to discuss the topic within the framework of the imaginary time-step method.[32] We start with the TDHF single-particle equations

$$i\hbar\,|\dot{\psi}_\lambda(t)\rangle=\hat{h}(t)\,|\psi_\lambda(t)\rangle \quad \lambda=1,2,\ldots,A\ . \tag{A1}$$

In terms of the discretized time,

$$t_k=k\Delta t\ ,$$

the solution of Eq. (A1) at time step $k+1$ can be obtained from step k by,

$$|\psi_\lambda^{k+1}\rangle=\exp(-i/\hbar\Delta t\hat{h}^k)\,|\psi_\lambda^k\rangle\ , \tag{A2}$$

where $\hat{h}^k$ is the single-particle Hamiltonian of the kth iteration step. The imaginary time-step method consists of the transformation $\Delta t\rightarrow -i\Delta t$,

$$|\chi_\lambda^{k+1}\rangle=\exp[-\epsilon(\hat{h}^k-\epsilon_\lambda^k)]\,|\chi_\lambda^k\rangle\ , \tag{A3}$$

where $\epsilon=\Delta t/\hbar$, and we have taken out a trivial phase from $|\psi_\lambda^k\rangle$. For all practical purposes, the gradient iteration step corresponds to the first-order expansion of the exponential operator,

$$|\chi_\lambda^{k+1}\rangle=\mathcal{O}[\,|\chi_\lambda^k\rangle-\epsilon(\hat{h}^k-\epsilon_\lambda^k)\,|\chi_\lambda^k\rangle]\ . \tag{A4}$$

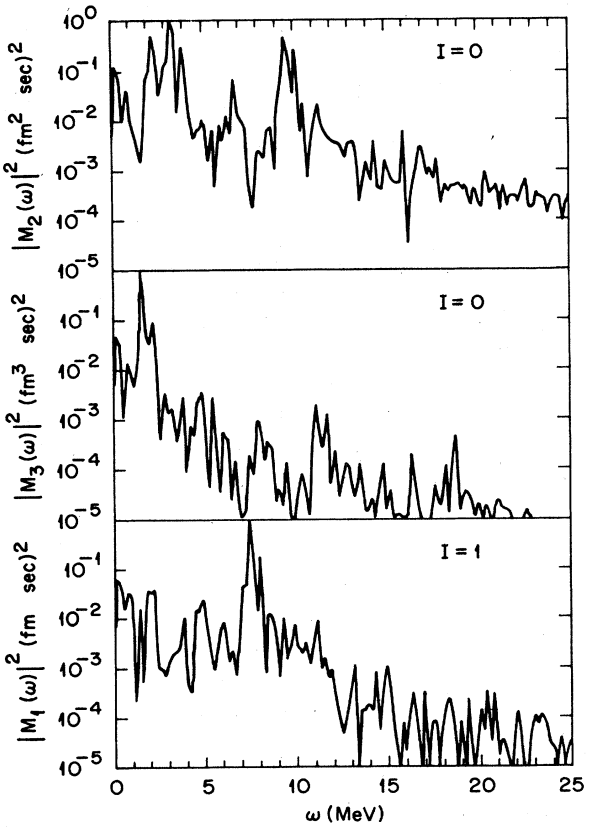

FIG. 8. The frequency dependence of the isoscalar quadrupole, isoscalar octupole, and the isovector dipole moments for the ^{24}Mg system from an initial configuration ^{4}He+^{20}Ne.

The operation of $\mathcal{O}$ denotes the necessary orthonormalization of the single-particle states. As is clearly seen from Eq. (A3), the exponential operator acts as a filter in selecting the lowest eigenvalues of $\hat{h}$ and leads to the minimization of the Hartree-Fock energy. Furthermore, the dampening parameter ϵ can be replaced by an operator $\hat{D}(k_0)$ to yield,

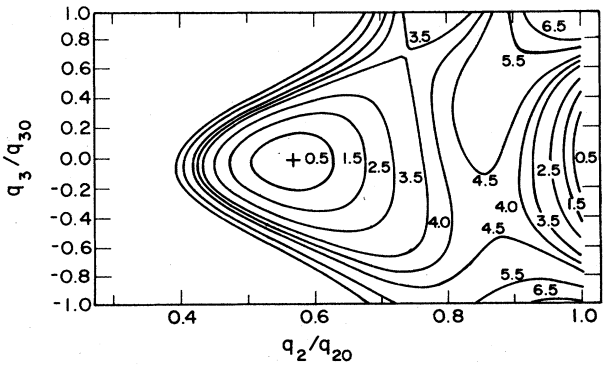

FIG. 9. Density constrained static Hartree-Fock energies. $E=E$(constrained) $-E_0$, $E_0=-122.3$ MeV, as a function of the isoscalar quadrupole and octupole degrees of freedom. Contours are labeled in MeV. The constants q_{20} and q_{30} are $q_{20}=56.6$ fm^2 and $q_{30}=-412.6$ fm^3. The point having the energy E_0 is a shape isomer of the ^{18}O system.

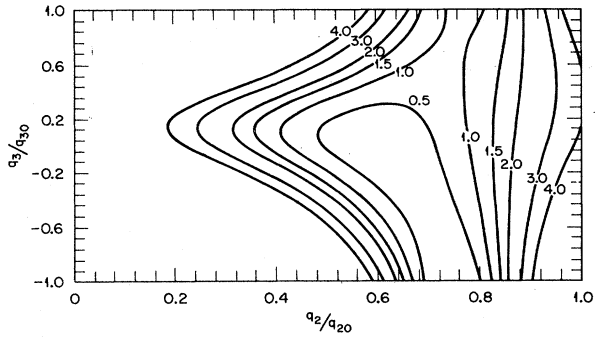

FIG. 10. Density constrained static Hartree-Fock energies. $E=E$ (constrained) $-E_0$, $E_0=-143.8$ MeV, as a function of the isoscalar quadrupole and octupole degrees of freedom. Contours are labeled in MeV. The constants q_{20} and q_{30} are $q_{20}=367.6$ fm^2 and $q_{30}=2164.3$ fm^3. The point having the energy E_0 is a shape isomer of the ^{24}Mg system.

$$|\chi_\lambda^{k+1}\rangle=\mathcal{O}[\,|\chi_\lambda^k\rangle-\hat{D}(k_0)(\hat{h}^k-\epsilon_\lambda^k)\,|\chi_\lambda^k\rangle\,]\,. \tag{A5}$$

For $\hat{D}(k_0)$ we choose,

$$\hat{D}(k_0)=\epsilon(1+\hat{T}/k_0)^{-1}\,. \tag{A6}$$

Here $\hat{T}$ is the kinetic energy operator defined on the spatial mesh points. This choice for $\hat{D}$ is motivated by the fact that the high-energy components for $\hat{h}$ will be dominated by the eigenvalues of the kinetic energy operator. In Eq. (A6) $\epsilon=0.05$ and k_0 fixes the energy damping scale. In all of our calculations we had $k_0=40$ MeV.

The convergence of the method is shown in Fig. 19 for three different nuclear configurations, ground state ^{20}Ne,

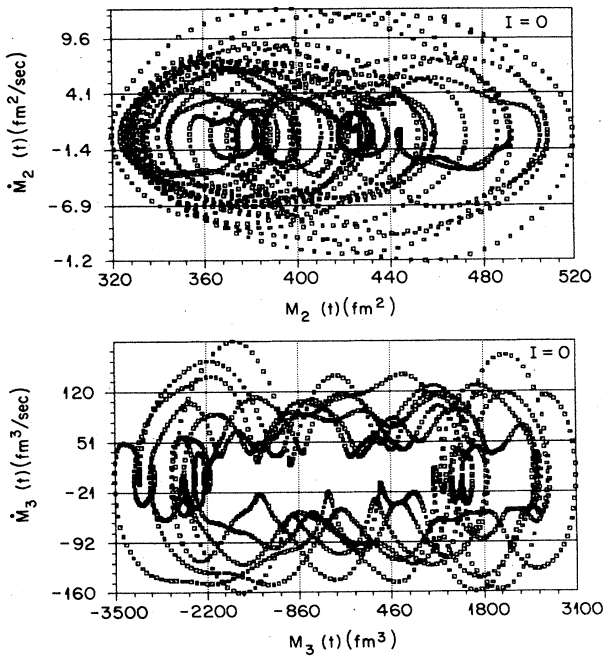

FIG. 11 Poincaré phases space plots of $\dot{M}_{LI}(t)$ vs $M_{LI}(t)$ for isoscalar quadrupole and isoscalar octupole modes for the ^{24}Mg system.

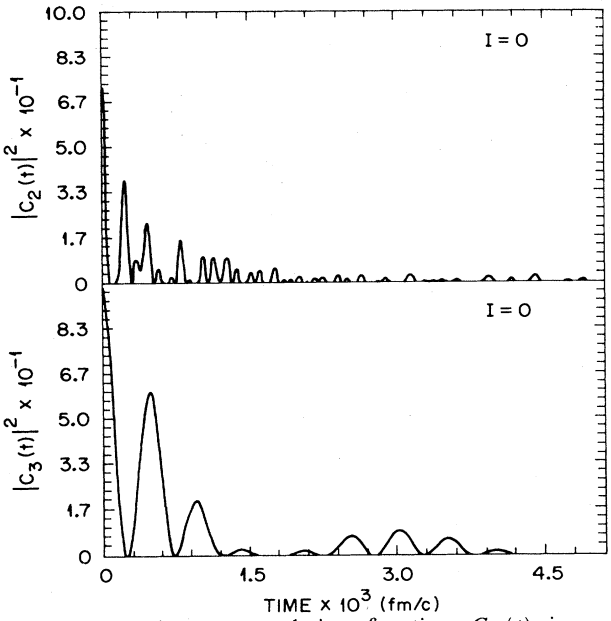

FIG. 12. The autocorrelation function $C_{LI}(t)$ in units MeV $(\mathrm{fm}^L\ \mathrm{sec})^2$ as a function of time for the isoscalar quadrupole and octupole modes in the ^{24}Mg system.

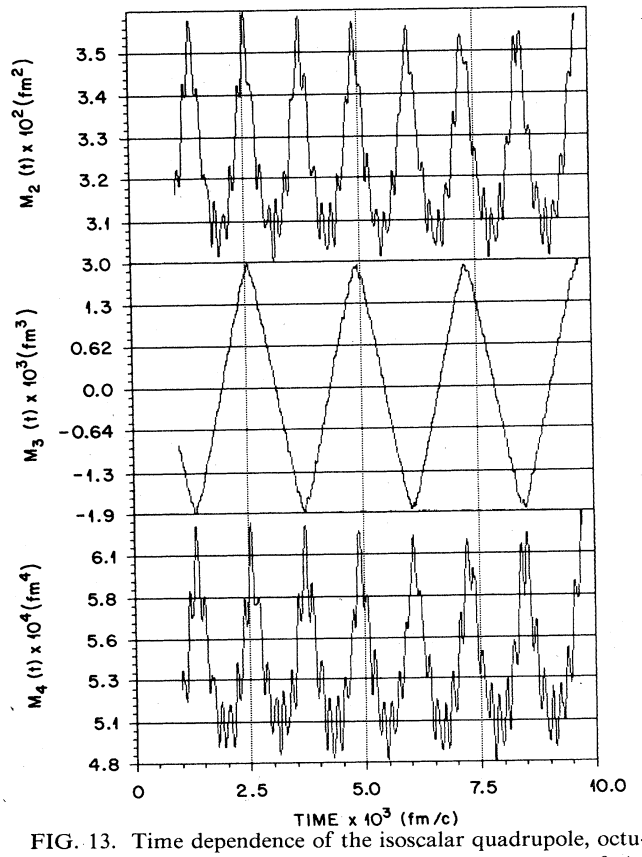

FIG. 13. Time dependence of the isoscalar quadrupole, octupole, and hexadecapole moments for the cooled modes of the ^{24}Mg system.

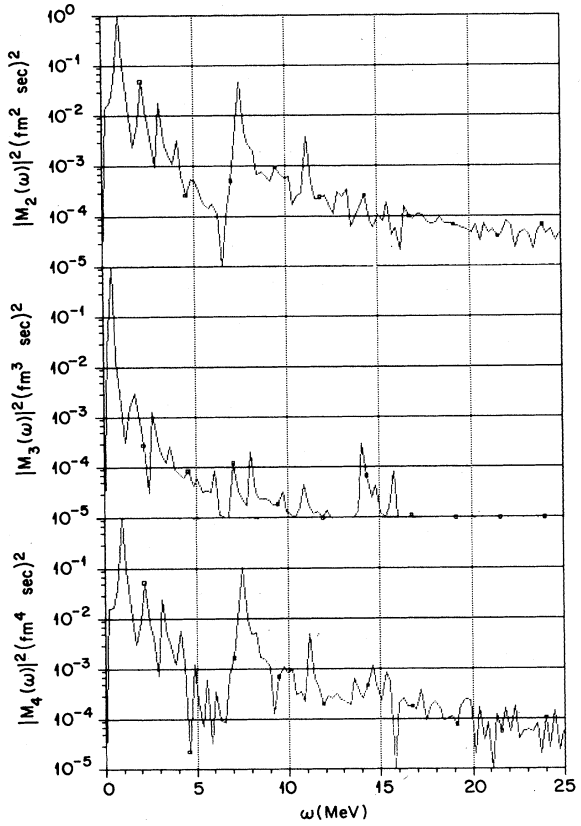

FIG. 14. Frequency dependence of the isoscalar quadrupole, octupole, and hexadecapole moments for the cooled modes of the ^{24}Mg system.

ground state ^{12}C, and the shape isomeric Hartree-Fock solution of ^{12}C(0^+). The ordinate of Fig. 19 shows the fractional change in the Hartree-Fock energy,

$$\Delta E^k = \frac{E^{k+1} - E^k}{E^k} \tag{A7}$$

as a function of the iteration number k. The Hartree-Fock iteration sequence is fully self-consistent, and the structure in the curve for ^{20}Ne results from a reordering of the single-particle states due to three separate shell crossings. This exponential convergence of the energy is a characteristic of the method and persists throughout the periodic table.

APPENDIX B

In Appendix A we have discussed the gradient iteration step for solving the static Hartree-Fock equations. Here, we will incorporate the constrained Hartree-Fock calculations into the gradient iteration step.[33] We will first illustrate the derivation for a general constraining field, and afterwards, we will write the equations for the density constraint. We start with an imaginary time iteration step of Eq. (A4),

$$|\chi_\lambda^{k+1}\rangle = \mathcal{O}[\,|\chi_\lambda^k\rangle - \epsilon(\hat{h}^k - \epsilon_\lambda^k)\,|\chi_\lambda^k\rangle\,] \,. \tag{B1}$$

It is possible to rewrite Eq. (B1) via the use of the projection operator,

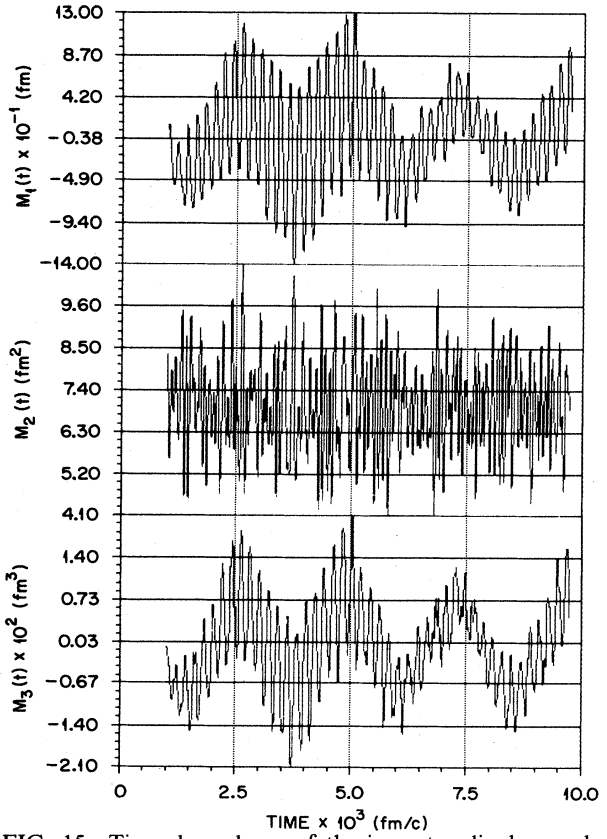

FIG. 15. Time dependence of the isovector dipole, quadrupole, and octupole moments for the cooled modes of the ^{24}Mg system.

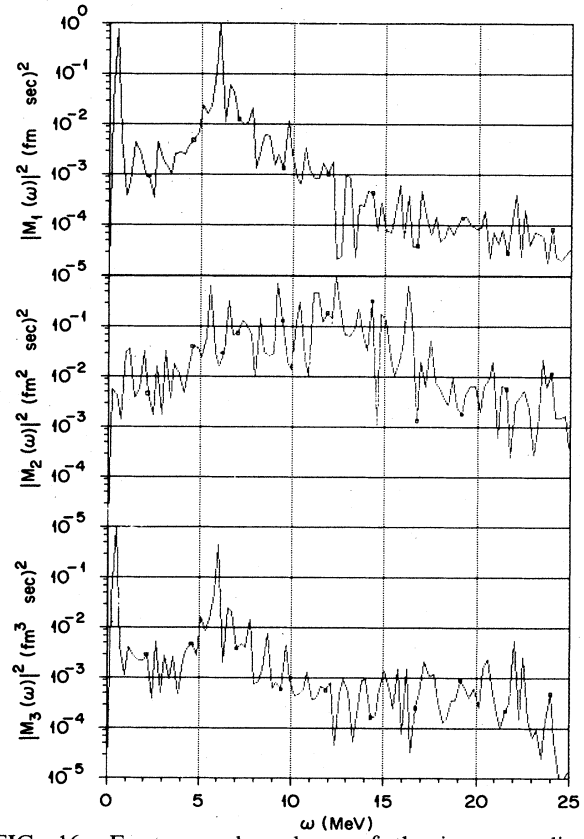

FIG. 16. Frequency dependence of the isovector dipole, quadrupole, and octupole moments for the cooled modes of the ^{24}Mg system.

$$\hat{P}^k_\lambda = 1 - |\chi^k_\lambda\rangle\langle\chi^k_\lambda| \tag{B2}$$

as,

$$|\chi^{k+1}_\lambda\rangle = \mathcal{O}(|\chi^k_\lambda\rangle - \epsilon\hat{P}^k_\lambda \hat{h}^k |\chi^k_\lambda\rangle) . \tag{B3}$$

The aim of this appendix is to devise an iteration scheme such that the expectation value of an arbitrary operator $\hat{Q}$ does not change from one iteration to the next.

$$\sum_\lambda \langle\chi^{k+1}_\lambda|\hat{Q}|\chi^{k+1}_\lambda\rangle = \sum_\lambda \langle\chi^k_\lambda|\hat{Q}|\chi^k_\lambda\rangle . \tag{B4}$$

Furthermore, we wish this expectation value to be equal to a fixed number Q_0. To achieve this, we use the method of Lagrange multipliers,

$$|\chi^{k+1}_\lambda\rangle = \mathcal{O}[|\chi^k_\lambda\rangle - \epsilon\hat{P}^k_\lambda(\hat{h}^k + \lambda\hat{Q})|\chi^k_\lambda\rangle] , \tag{B5}$$

where λ is to be determined from Eq. (B4). The application of the Gram-Schmidt orthogonalization procedure yields, to order ϵ^2,

$$|\chi^{k+1}_\lambda\rangle = (1-\hat{A}_\lambda)|\chi^k_\lambda\rangle + \sum_{\mu=1}^{\lambda-1}(\langle\chi^k_\lambda|\hat{A}^\dagger_\lambda|\chi^k_\mu\rangle + \langle\chi^k_\lambda|\hat{A}_\mu|\chi^k_\mu\rangle)|\chi^k_\mu\rangle , \tag{B6}$$

where we have defined,

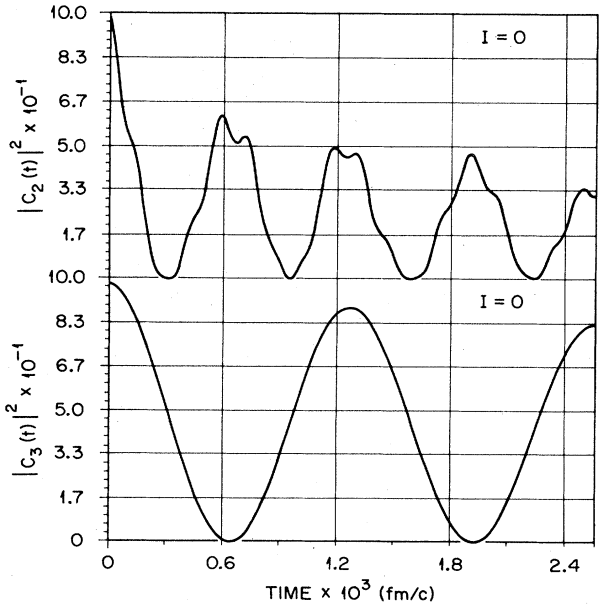

FIG. 17. The autocorrelation function $C_{LI}(t)$ in units MeV(fm^L sec)^2 as a function of time for the isoscalar quadrupole and octupole moments for the cooled modes of ^{24}Mg.

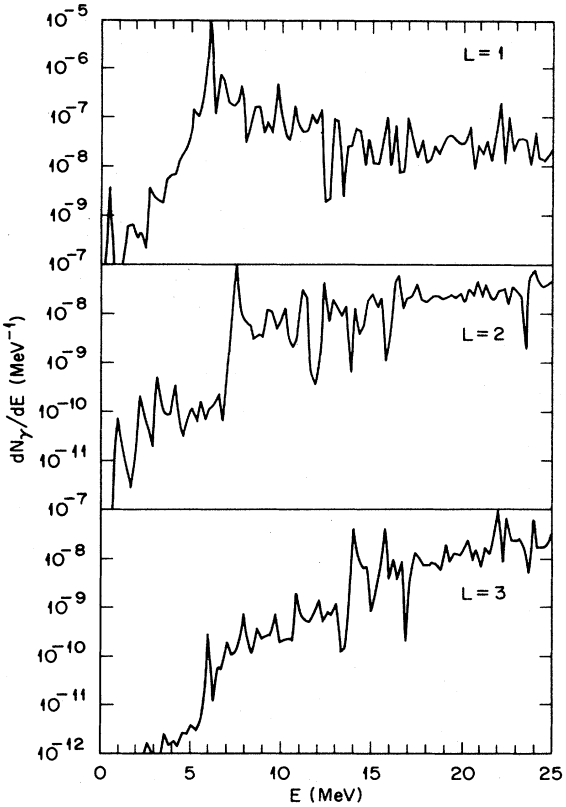

FIG. 18. The γ spectrum, dN_γ/dE (MeV^{-1}), as a function of the γ energy, E (MeV), for the cooled modes of the ^{24}Mg system.

$$\hat{A}_\lambda = \hat{P}^k_\lambda \epsilon (\hat{h}^k + \lambda \hat{Q}) \ . \tag{B7}$$

From Eq. (B6) we calculate the left-hand side of Eq. (B4) to obtain,

$$\lambda = \frac{\langle x \mid \hat{Q}(\hat{h}^k + \lambda \hat{Q}) \mid x \rangle}{\langle x \mid \hat{Q}^2 \mid x \rangle} \ , \tag{B8}$$

where

$$\langle x \mid \hat{A}\hat{B} \mid x \rangle = \sum_\lambda \langle \chi^k_\lambda \mid \hat{A}\hat{B} \mid \chi^k_\lambda \rangle - 2 \sum_\lambda \sum_{\mu=1}^{\lambda-1} \langle \chi^k_\lambda \mid \hat{A} \mid \chi^k_\mu \rangle \langle \chi^k_\mu \mid \hat{B} \mid \chi^k_\lambda \rangle \ . \tag{B9}$$

The difference between the expectation value of $\hat{Q}$ in each iteration step will be of order ϵ^2. To further correct for this error, we add a term which is solely driven by this difference,

$$\delta\lambda = \frac{\left[\sum_\lambda \langle \chi^k_\lambda \mid \hat{Q} \mid \chi^k_\lambda \rangle - Q_0 \right] \Big/ 2\epsilon}{\langle x \mid \hat{Q}^2 \mid x \rangle} \ . \tag{B10}$$

This is then the most optimal value of λ to be used at each iteration step. As we see, the calculation of the exchange terms is rather costly. Instead, it is possible to formulate an iterative scheme for determining λ at each

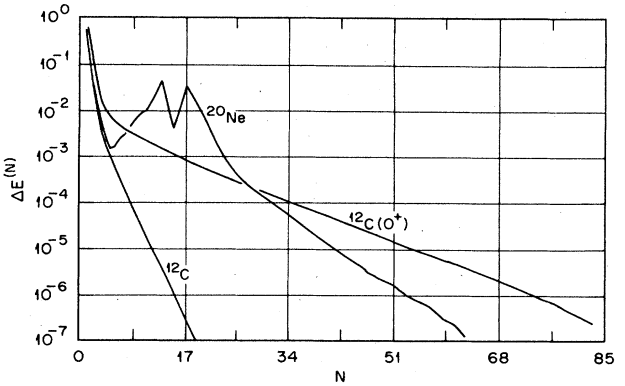

FIG. 19. Convergence of the gradient iteration method for the nuclei ^{12}C, ^{12}C(0$^+$), and ^{20}Ne. The structure in the ^{20}Ne curve arises from the reordering of the single-particle states due to three separate shell crossings.

iteration step. To do this, we perform an intermediate step,

$$| \chi^{k+(1/2)}_\lambda \rangle = \mathcal{O}[\ | \chi^k_\lambda \rangle - \epsilon(\hat{h}^k + \lambda^k \hat{Q} - \epsilon^k_\lambda) \mid \chi^k_\lambda \rangle] \tag{B11}$$

and calculate the difference,

$$\delta Q^{k+(1/2)} = \sum_\lambda \langle \chi^{k+(1/2)}_\lambda \mid \hat{Q} \mid \chi^{k+(1/2)}_\lambda \rangle - \sum_\lambda \langle \chi^k_\lambda \mid \hat{Q} \mid \chi^k_\lambda \rangle \ . \tag{B12}$$

We then correct λ to reduce this difference,

$$\lambda^{k+1} = \lambda^k + C_0 \frac{\delta Q^{k+(1/2)}}{2\epsilon \sum_\lambda \langle \chi^k_\lambda \mid \hat{Q}^2 \mid \chi^k_\lambda \rangle + d_0} \ , \tag{B13}$$

where we have replaced the exchange term by the constant d_0. In terms of these intermediate states, the $(k+1)$th step is given by,

$$| \chi^{k+1}_\lambda \rangle = \mathcal{O}[\ | \chi^{k+(1/2)}_\lambda \rangle - \epsilon(\lambda^{k+1} - \lambda^k + \delta\lambda^k) \hat{Q} \mid \chi^{k+(1/2)}_\lambda \rangle] \ , \tag{B14}$$

where

$$\delta\lambda^k = \frac{\sum \langle \chi^k \mid \hat{Q} \mid \chi^k \rangle - Q_0}{2\epsilon \sum_\lambda \langle \chi^k_\lambda \mid \hat{Q}^2 \mid \chi^k_\lambda \rangle + d_0} \ . \tag{B15}$$

The extension of this method to the density constraints is a trivial one. In this case, we would like to constrain a continuous density,

$$\rho^k(r) = \sum_\lambda | \chi^k_\lambda(r) |^2 \tag{B16}$$

to be equal to $\rho_0(r)$. The operator $\hat{Q}$ becomes the density operator $\hat{\rho}(r)$ defined as,

$$\langle \chi^k_\lambda \mid \hat{\rho}(r) \mid \chi^k_\lambda \rangle = | \chi^k_\lambda(r) |^2 \tag{B17}$$

and the product $\lambda\hat{Q}$ becomes an integral,

$$\lambda \hat{Q} \rightarrow \int d^3r \, \lambda(r) \hat{\rho}(r) \ . \tag{B18}$$

Note that in coordinate space $\hat{\rho}(r)$ is a delta function, and

$$\int d^3r\, \lambda(r)\hat{\rho}(r)=\lambda(r)\ . \tag{B19}$$

From these equations the iterative scheme for $\lambda^k(r)$ can be written as

$$\lambda^{k+1}(r)=\lambda^k(r)+C_0\frac{\delta\rho^{k+(1/2)}}{2\epsilon\rho^k(r)+d_0}\ , \tag{B20}$$

where

$$\delta\rho^{k+(1/2)}(r)=\rho^{k+(1/2)}(r)-\rho_0(r) \tag{B21}$$

is obtained from the half-time iteration step,

$$|\chi_\lambda^{k+(1/2)}\rangle=\mathcal{O}[\,|\chi_\lambda^k\rangle-\epsilon(\hat{h}^k+\lambda^k(r)-\epsilon_\lambda^k)\,|\chi_\lambda^k\rangle\,]\ . \tag{B22}$$

Using these wave functions, the $(k+1)$th iteration becomes

$$|\chi_\lambda^{k+1}\rangle=\mathcal{O}\{\,|\chi_\lambda^{k+(1/2)}\rangle -\epsilon[\lambda^{k+1}(r)-\lambda^k(r)+\delta\lambda^k(r)]\,|\chi_\lambda^{k+(1/2)}\rangle\}\ , \tag{B23}$$

where

$$\delta\lambda^k(r)=c_0\frac{\rho^k(r)-\rho_0(r)}{2\epsilon\rho_0(r)+d_0}\ .$$

In practical calculations the parameter ϵ of Eq. (B1) has been replaced by the damping operator of Eq. (A6), and the constants c_0 and d_0 were chosen to be 0.9 and 7×10^{-5}, respectively.

*Present address: Institut für Theoretische Physik, Universität Erlangen, D-8520 Erlangen, Federal Republic of Germany.

[1]A. K. Kerman and S. E. Koonin, Ann. Phys. (N.Y.) **100**, 332 (1976).
[2]S. E. Koonin, Prog. Part. Nucl. Phys. **4**, 283 (1979).
[3]J. W. Negele, Rev. Mod. Phys. **54**, 913 (1982).
[4]K. T. R. Davies, K. R. S. Devi, S. E. Koonin, and M. R. Strayer, in *Treatise on Heavy-Ion Science,* edited by D. A. Bromley (Plenum, New York, 1985), Vol. 3.
[5]K. T. R. Davies and S. E. Koonin, Phys. Rev. C **23**, 2042 (1981).
[6]P. Bonche, S. E. Koonin, and J. W. Negele, Phys. Rev. C **13**, 1226 (1976).
[7]S. E. Koonin, K. T. R. Davies, V. Maruhn-Rezwani, H. Feldmeier, S. J. Krieger, and J. W. Negele, Phys. Rev. C **15**, 1359 (1977).
[8]F. Villars, Nucl. Phys. **A285**, 369 (1977).
[9]M. Baranger and M. Veneroni, Ann. Phys. (N.Y.) **114**, 123 (1978).
[10]M. J. Giannoni and P. Quentin, Phys. Rev. C **21**, 2060 (1980).
[11]K. Goeke, P.-G. Reinhard, and D. J. Rowe, Nucl. Phys. **A359**, 408 (1981).
[12]K. Goeke, P.-G. Reinhard, and H. Reinhardt, Nucl. Phys. **A378**, 474 (1982).
[13]K. Goeke, F. Grummer, and P.-G. Reinhard, Ann. Phys. (N.Y.) **150**, 504 (1983).
[14]C. W. Wong, Phys. Rep. **15**, 283 (1975).
[15]P.-G. Reinhard, K. Goeke, and R. Y. Cusson, in *Time-Dependent Hartree-Fock and Beyond,* edited by K. Goeke and P.-G. Reinhard (Springer, New York, 1982).
[16]S. Levit, Phys. Rev. C **21**, 1594 (1980).
[17]S. Levit, J. W. Negele, and Z. Paltiel, Phys. Rev. C **21**, 1603 (1980).
[18]J. P. Blaizot, Phys. Lett. **107B**, 331 (1981).
[19]J. P. Blaizot and G. Ripka, Phys. Lett. **105B**, 1 (1981).
[20]I. Zahed and M. Baranger, Phys. Rev. C **29**, 1010 (1984).
[21]R. H. G. Helleman, Nordisk Institut für Theoretisk Atomfysik report 1981, p. 165.
[22]E. Fermi, J. Pasta, and S. Ulam, Los Alamos Scientific Laboratory Report LA-1940, 1957.
[23]A. K. Kerman and S. Levit, Phys. Rev. C **24**, 1029 (1981).
[24]Y. Alhassid and S. E. Koonin, Phys. Rev. C **23**, 1590 (1981).
[25]G. Bertsch, Nucl. Phys. **A249**, 253 (1975).
[26]D. Ruelle, Math. Intellegencer **2**, 126 (1980).
[27]J. Błocki and H. Flocard, Phys. Lett. **85B**, 163 (1979).
[28]R. Y. Cusson, H. Stöcker, M. R. Strayer, A. S. Umar, D. A. Bromley, J. A. Maruhn, and W. Greiner, in *Time-Dependent Hartree-Fock and Beyond,* edited by K. Goeke and P.-G. Reinhard (Springer, New York, 1982).
[29]M. R. Strayer, R. Y. Cusson, A. S. Umar, P.-G. Reinhard, D. A. Bromley, and W. Greiner, Phys. Lett. **135B**, 261 (1984).
[30]M. R. Strayer, in *Fusion Reactions Below the Coulomb Barrier,* edited by S. G. Steadman (Springer, New York, 1984).
[31]P.-G. Reinhard and R. Y. Cusson, Nucl. Phys. **A378**, 418 (1982).
[32]K. T. R. Davies, H. Flocard, S. Krieger, and M. S. Weiss, Nucl. Phys. **A342**, 111 (1980).
[33]R. Y. Cusson, P.-G. Reinhard, M. R. Strayer, J. A. Maruhn, and W. Greiner, Z. Phys. A **320**, 475 (1985).
[34]L. D. Landau and E. M. Lifshitz, *The Classical Theory of Fields* (Pergamon, New York, 1979), p. 66.
[35]J. D. Jackson, *Classical Electrodynamics* (Wiley, New York, 1975), p. 739.
[36]K. A. Erb and D. A. Bromley, Phys. Rev. C **23**, 2781 (1981).
[37]G. Leander and S. E. Larsson, Nucl. Phys. **A239**, 93 (1975).
[38]G. Ahlers and R. P. Behringer, Prog. Theor. Phys. Suppl. **64**, 106 (1980).
[39]R. H. G. Helleman, in *Nonlinear Dynamics and the Beam-Beam Interaction (Brookhaven National Laboratory, 1979),* Proceedings of the Symposium on Nonlinear Dynamics and the Beam-Beam Interaction, AIP Conf. Proc. No. **57**, edited by M. Month and J. C. Herrera (AIP, New York, 1979), p. 236.
[40]*Intrinsic Stochasticity in Plasmas,* edited by G. Laval and D. Gresillen (Les Editions de Physique, Orsay, France, 1980).
[41]R. D. Williams and S. E. Koonin, Nucl. Phys. **A391**, 72 (1982).
[42]S. Y. Li, A. Klein, and R. M. Dreizler, J. Math, Phys. **11**, 975 (1970).